INTERNATIONAL JOURNAL FOR NUMERICAL METHODS IN FLUIDS
Int. J. Numer. Meth. Fluids 2005; **48**:423–454
Published online 14 February 2005 in Wiley InterScience (www.interscience.wiley.com). DOI: 10.1002/fld.932

Some issues regarding spectral element meshes for moving journal bearing systems

D. Rh. Gwynllyw[1,*,†] and T. N. Phillips[2,‡]

[1]*School of Mathematical Sciences, University of the West of England, Bristol BS16 1QY, U.K.*
[2]*School of Mathematics, Cardiff University, Cardiff CF24 4AG, U.K.*

SUMMARY

This paper concerns the modelling of dynamically loaded journal bearing systems using a moving spectral element method. The moving grid method employed in this paper is the arbitrary Lagrangian–Eulerian (ALE) method. The ALE methodology is compared with a quasi-Eulerian approach in the context of dynamically loaded journal bearings and the advantages of adopting the ALE formulation are highlighted. A comparison with the predictions of lubrication theory is also presented and the limitations of the lubrication approximation are demonstrated when inertial effects are significant. A comprehensive set of results is presented illustrating the salient features of the spectral element mesh generation schemes described in the paper and the way in which these impinge on the efficiency of the iterative solution of the discrete equations at each time step. Copyright © 2005 John Wiley & Sons, Ltd.

KEY WORDS: dynamically loaded journal bearings; spectral element method; ALE formulation

1. INTRODUCTION

Most problems in Newtonian fluid mechanics are expressed using the Eulerian formulation in which the reference system is fixed in space. Discretization methods for problems posed using this formulation use points (finite difference schemes) or elements (finite element schemes) fixed in space. If the boundary of the domain moves as it does in moving boundary problems, then difficulties can arise when the boundary is not aligned to the finite difference mesh or a side of a finite element. This necessitates the use of an interpolation scheme to impose the conditions.

On the other hand, the Lagrangian formulation, which is widely used in solid mechanics applications, uses a reference system that is associated with material particles. Excessive

*Correspondence to: D. Rh. Gwynllyw, School of Mathematical Sciences, University of the West of England, Bristol BS16 1QY, U.K.
†E-mail: Rhys.Gwynllyw@uwe.ac.uk
‡E-mail: phillipsTN@cardiff.ac.uk

Received 23 June 2004
Revised 2 December 2004
Accepted 6 December 2004

particle movement can present problems such as distortion of finite elements. In this situation, in order to avoid deterioration in accuracy, the underlying finite element mesh needs to be regenerated (remeshing) with interpolation used to transfer variables from the old to the new mesh.

The shortcomings of pure Lagrangian and Eulerian descriptions prompted the development of what are known as arbitrary Lagrangian–Eulerian techniques. These methods utilize the advantages of both the Lagrangian and Eulerian formulations whilst at the same time avoiding their drawbacks. The ALE method was first proposed in the finite difference context by Hirt *et al.* [1] and Noh [2]. In the 1980s, the method was developed for finite element applications by Donea *et al.* [3] and Belytschko *et al.* [4]. The ALE approach is based on the arbitrary movement of the reference frame, i.e. the reference system is not fixed a priori in space or associated with the fluid. It may be considered as a computational reference system that can be chosen quite arbitrarily and which is continually changing in order to allow for the precise description of moving interfaces and to ensure the integrity of the mesh over time.

There are alternative methods that could be used for performing numerical simulations of problems involving a computational domain that is evolving in time. For example, there is the space–time finite element method developed by Hughes and Hulbert [5] and Tezduyar *et al.* [6, 7]. In this approach, the temporal as well as the spatial coordinate is discretized using finite element methods. The deformation of the spatial domain in time is reflected through the deformation of the mesh in the temporal co-ordinate. An advantage of this approach is its generality. It is possible to view the ALE finite element method as a special case of the space–time method (see Reference [8], for example).

The distributed Lagrangian multiplier (DLM) particle mover has also been developed by Glowinski *et al.* [9] to simulate fluid–solid systems. The basic idea behind the DLM particle mover is to extend a problem defined on a time-dependent geometrically complex domain to a stationary, larger but simpler domain known as the fictitious domain. On this fictitious domain, the constraints of rigid body motion of the particles are enforced using a distributed Lagrange multiplier, which represents the additional body force required to maintain the rigid body motion inside the particle.

Finally, a completely different approach is based on the lattice Boltzmann method (LBM). Unlike conventional numerical schemes based on discretizations of macroscopic continuum equations, LBM is based on microscopic models and mesoscopic kinetic equations. The idea underlying LBM is to construct simplified kinetic theory models that incorporate the essential physics of the microscopic or mesoscopic processes so that the macroscopic-averaged properties obey the desired macroscopic equations. A full account of LBM may be found in the monograph of Succi [10].

The development of the ALE technique to simulate the motion of particles in fluids is due to Hu and co-workers [11, 12]. The method has been used to solve problems involving both Newtonian and viscoelastic fluids in two-dimensional and three-dimensional geometries. In a more recent paper Hu *et al.* [13] introduced a combined weak formulation incorporating both the fluid and particle equations of motion. The advantage of this approach is that the hydrodynamic forces and moments on the particles do not need to be computed explicitly, thus contributing to a more stable scheme.

An implementation of ALE within the spectral element context was originally proposed by Ho and Patera [14, 15] who used the technique to simulate free surface flows. The spectral element approximation introduces high-order accuracy into the spatial discretization. In this

paper we use this combination to perform direct numerical simulations of the motion of a moving journal bearing system.

Two distinct moving journal bearing systems are considered in this paper, namely the dynamically loaded journal bearing (DLJ) and the journal bearing simulator (JBS). The dynamically loaded journal bearing is a system whereby the journal rotates about its own centre at a given angular velocity but whose axis is free to move under the forces imparted on the journal. These forces are a combination of hydrodynamic forces and prescribed external applied loads. In contrast, the journal bearing simulator is a system whereby the journal's path is prescribed and is not dependent upon the hydrodynamic forces.

The paper is organized as follows. In Section 2 the governing equations for a generalized Newtonian fluid are introduced and the viscosity law is described. In Section 3 the dynamically loaded journal bearing problem is defined. An analysis of the problem using lubrication theory is described in Section 4, with particular reference to the influence of inertia. The spectral element discretization is described in Section 5 together with iterative methods for solving the spectral element equations at each time step. The quasi-Eulerian (QE) and ALE strategies for moving the mesh are described in Section 6. An implicit algorithm for determining the motion of the journal is discussed in Section 7 and strategies for generating the computational grid are described in Section 8. Numerical results comparing the efficiency of the preconditioners for solving the linear system of equations generated by the spectral element method and the strategies for mesh generation and movement are presented in Section 9. A comparison between predictions obtained using direct numerical simulations using the ALE formulation and those obtained using lubrication theory is also given in Section 9. Finally, concluding remarks are provided in Section 10.

2. GOVERNING EQUATIONS

The governing equations for an incompressible inelastic fluid comprise the conservation of momentum

$$\rho\left(\frac{\partial \boldsymbol{v}}{\partial t}+\boldsymbol{v}\cdot\nabla\boldsymbol{v}\right)=-\nabla p+\nabla\cdot\boldsymbol{\tau}+\mathbf{b} \tag{1}$$

the conservation of mass

$$\nabla\cdot\boldsymbol{v}=0 \tag{2}$$

and the constitutive equation

$$\boldsymbol{\tau}=2\eta(\dot{\gamma},p)\mathbf{d} \tag{3}$$

where $\boldsymbol{v}$ represents fluid velocity, p is the pressure, ρ is the density, η is the variable viscosity, $\mathbf{b}$ is a body force, $\dot{\gamma}=\sqrt{2\,\mathrm{tr}(\mathbf{d}^2)}$ is the generalized shear-rate, $\boldsymbol{\tau}$ is the deviatoric stress tensor and $\mathbf{d}=\frac{1}{2}(\nabla\boldsymbol{v}+(\nabla\boldsymbol{v})^{\mathrm{T}})$ is the rate of deformation tensor. In non-Newtonian fluid mechanics the deviatoric stress tensor is more commonly known as the extra-stress tensor and it is this terminology that will be adopted for the rest of this paper. Here $\mathrm{tr}(\mathbf{A})$ denotes the trace of a tensor $\mathbf{A}$. The generalized shear-rate reduces to the shear-rate in a pure shear flow. The constitutive equation (3) is a modification of the usual generalized Newtonian model to include pressure dependence of the viscosity.

The viscosity law that we have used was proposed by Davies and Li [16]. It is shear-thinning and pressure-thickening. The various parameters in the model are determined empirically. The dependence of viscosity on $\dot{\gamma}$ and pressure is given by

$$\eta(\dot{\gamma}, p) = \left\{ \eta_\infty + \frac{(\eta_0 - \eta_\infty)}{[1 + (\kappa\dot{\gamma})^m]} \right\} \times \exp(-\alpha \operatorname{tr}(\boldsymbol{\sigma})/3 + F) \tag{4}$$

where κ is a function of pressure

$$\kappa = \kappa(p) = \exp(-\bar{\alpha} \operatorname{tr}(\boldsymbol{\sigma})/3 + E)$$

$\boldsymbol{\sigma} = -p\mathbf{I} + \boldsymbol{\tau}$ is the Cauchy stress tensor and $\eta_0, \eta_\infty, m, n, \alpha, \bar{\alpha}$, E and F are material parameters. This model describes the shear-thinning behaviour of the viscosity by a Cross-type formula. Pressure-thickening is modelled by a simple exponential law [17]. It is important to note that the viscosity law (4) is consistent with experiments [18] which span only limited ranges of the pressures which the lubricants experience under general operating conditions.

3. DYNAMICALLY LOADED JOURNAL BEARING PROBLEM

Consider the two-dimensional geometry shown schematically in Figure 1. The journal of radius R_J rotates with a predetermined constant angular velocity ω about its own centre whilst moving with a time-dependent translational velocity $\boldsymbol{v}_J$. The journal's motion is lubricated by a fluid lubricant contained within a stationary bearing of radius R_B. Both the journal and the bearing are assumed to be of infinite extent in the axial z-direction. The time-dependent eccentricity of the system is denoted by e, with the eccentricity ratio defined by

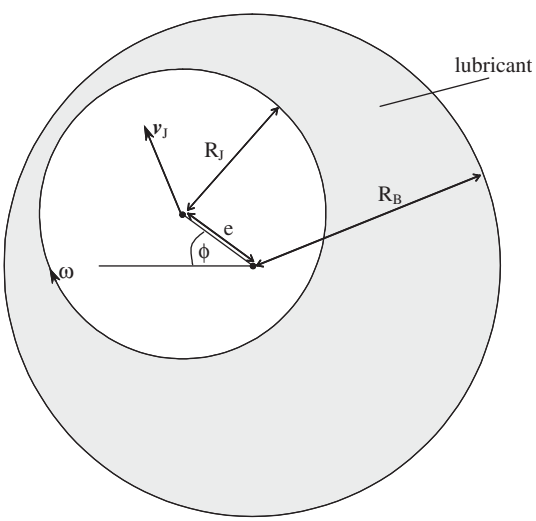

Figure 1. Schematic diagram of the dynamically loaded journal bearing system.

$\varepsilon = e/c$, $0 \leqslant \varepsilon \leqslant 1$, where $c = R_B - R_J$ is the average gap. The attitude angle of the journal is denoted by ϕ.

The motion of the journal is determined by the forces acting upon it with contributions from a prescribed applied load (which may be time-dependent), the journal's own weight, and the hydrodynamic force exerted on the journal by the lubricant. The result is that the centre of the journal traces out a non-trivial path in space.

The lubricant satisfies the governing equations (1)–(3) which are solved subject to specified boundary and initial conditions. These are, respectively,

$$\boldsymbol{v}(\mathbf{x}, t) = \boldsymbol{v}_J(t) \text{ with } \mathbf{x} \in \Gamma_J, \quad \boldsymbol{v}(\mathbf{x}, t) = \mathbf{0} \text{ with } \mathbf{x} \in \Gamma_B \tag{5}$$

$$\boldsymbol{v}(\mathbf{x}, t = 0) = \boldsymbol{v}_0(\mathbf{x}) \tag{6}$$

where Γ_J and Γ_B denote the boundaries of the journal and bearing, respectively. The initial velocity profile, $\boldsymbol{v}_0(\mathbf{x})$, is the steady state solution of Equations (1)–(3) subject to the appropriate boundary conditions. This ensures that mass is conserved globally.

4. LUBRICATION THEORY

The use of lubrication theory is the most popular approach for the analysis of dynamically loaded journal bearings. In such methods the modelling of the fluid is based upon the Reynolds equation which assumes a small gap in the journal bearing geometry. Certain terms in the Reynolds equation can be eliminated using either the long or short bearing approximation leading to a simplification of the governing equations.

A number of important fluid properties have been incorporated into the study of lubrication theory for dynamically loaded journal bearings. These include the issues of inertia, non-Newtonian effects both in terms of shear-thinning and viscoelasticity, cavitation and elastohydrodynamic lubrication. See, for example, [19–21]. Both analytical and numerical methods have been applied to the solution of the Reynolds equation in the context of dynamically loaded journal bearings.

Collins *et al.* [22] investigated the stabilizing effects of inertia on the dynamically loaded journal bearing. Using the Reynolds equation for a full film, a coupled system of second-order differential equations was obtained for the motion of the journal. The solution of this system enabled characteristic neutral stability curves to be drawn. A weakly nonlinear stability analysis in the operational vicinity of the neutral stability curves determined the existence of stable, small-amplitude limit cycles.

In the current work, the equations of motion for the journal, developed by Collins *et al.* [22], are numerically integrated to obtain the locus of the journal under different operating conditions. These results are compared with the journal locus calculations obtained by using the spectral element method to model the full governing equations of the fluid (1)–(3).

Using the assumptions of lubrication theory, Collins *et al.* [22] obtained the following expressions for the tangential and radial components of the hydrodynamic force, (F_t, F_r), up to

terms of order λ:

$$\alpha F_t = \frac{12\pi(1-2\phi')\varepsilon}{(2+\varepsilon^2)(1-\varepsilon^2)^{1/2}} + \lambda\pi\left\{\frac{6\varepsilon'(1-2\phi')}{35(2+\varepsilon^2)^3}\{3(26-\varepsilon^2)(2+\varepsilon^2) + (1-\varepsilon^2)^{1/2}(\varepsilon^4+36\varepsilon^2-100)\} + \frac{12\phi''}{5\varepsilon(2+\varepsilon^2)^2}\{(2+\varepsilon^2)(2-5\varepsilon^2)-4(1-\varepsilon^2)^{3/2}\}\right\} \tag{7}$$

$$\alpha F_r = \frac{-12\pi\varepsilon'}{(1-\varepsilon^2)^{1/2}} - \lambda\pi\left\{\frac{3\varepsilon(1-2\phi')^2}{35(2+\varepsilon^2)^2}[3(2+\varepsilon^2)-(1-\varepsilon^2)^{1/2}(20+\varepsilon^2)] + \frac{1-(1-\varepsilon^2)^{1/2}}{5\varepsilon} - \frac{6\varepsilon'^2}{5\varepsilon^3}\left[2-\frac{(2-\varepsilon^2)}{(2-\varepsilon^2)^{1/2}}\right] + \frac{12\varepsilon''}{5\varepsilon^2}[1-(1-\varepsilon^2)^{1/2}]\right\} \tag{8}$$

where $\lambda = c/R_J\,\mathrm{Re}$, $\mathrm{Re} = \rho c R_J \omega/\eta$, $\alpha = c^2/\omega\eta R_J^3$, and the prime denotes differentiation with respect to $\tau = \omega t$.

In the dynamically loaded journal bearing, the bearing moves under the influence of the hydrodynamic forces and an applied load, $\boldsymbol{S} = (S_x, S_y)$. The motion of the journal can therefore be determined using the equation of motion:

$$m\ddot{\mathbf{r}} = \boldsymbol{F} = (F_r\cos\phi + F_t\sin\phi + S_x, -F_r\sin\phi - F_t\cos\phi + S_y) \tag{9}$$

where $\mathbf{r}$ is the position vector of the centre of the journal and the double dot denotes differentiation twice with respect to t.

Both the right-hand and left-hand sides of (9) contain terms in e'', ϕ'' and these can be isolated on the left-hand side to obtain

$$\begin{pmatrix} e'' \\ \phi'' \end{pmatrix} = \frac{1}{\Delta}\begin{pmatrix} (F_2-\beta e)\cos\phi & -(\beta e - F_2)\sin\phi \\ -(F_1-\beta)\sin\phi & (F_1-\beta)\cos\phi \end{pmatrix} \times \left\{\begin{pmatrix} -G_1\cos\phi + G_2\sin\phi - F \\ -G_2\cos\phi - G_1\sin\phi \end{pmatrix} + \beta\begin{pmatrix} -2e'\phi'\sin\phi - e\phi'^2\cos\phi \\ 2e'\phi'\cos\phi - e\phi'^2\sin\phi \end{pmatrix}\right\} \tag{10}$$

where

$$F_r = e''F_1 + G_1, \quad F_1 = F_1(\alpha,\lambda,\varepsilon), \quad G_1 = G_1(\alpha,\lambda,\varepsilon,\varepsilon'\phi')$$
$$F_t = \phi''F_2 + G_2, \quad F_2 = F_2(\alpha,\lambda,\varepsilon), \quad G_2 = G_2(\alpha,\lambda,\varepsilon,\varepsilon'\phi')$$

Under the lubrication theory assumptions, this paper considers two approaches to calculate the motion of the journal. In the first approach the Cartesian acceleration vector is obtained from (9), with the velocity and locus of the journal obtained by numerical integration of the ODE. Note that the right-hand side of (9) contains terms involving second derivatives which are taken as the values at the previous time-step. In the second approach, Equation (10) is

solved to obtain the ordered pair $(\ddot{e}, \ddot{\phi})$ and, following numerical integration, the velocity and locus of the journal. In Equation (10) all second derivatives have been isolated on the left-hand side of the equation.

5. THE SPECTRAL ELEMENT METHOD

5.1. Temporal discretization

We first consider the temporal discretization of the equations for a statically loaded journal bearing. The temporal scheme for the dynamically loaded journal bearing will incorporate elements of the static scheme at each time step within an iterative scheme for the movement of the journal. The temporal discretization for the dynamically loaded case is described in Section 7.

A number of semi-discrete schemes were considered for the transient discretization of the fluid's governing equation. Under consideration were the implicit Euler scheme, an Adams Moulton/Bashforth type scheme and a Gear backward differentiation scheme. All the schemes come under the general description of the following semi-discrete system:

$$\rho\left(\frac{\boldsymbol{F}_{(n+1),(n),(n-1)}}{\Delta t} + \boldsymbol{C}_{(n+1),(n),(n-1)}\right) = \boldsymbol{L}_{(n+1),(n)} \tag{11}$$

$$\nabla \cdot \boldsymbol{v}^{(n+1)} = 0 \tag{12}$$

$$\boldsymbol{\tau}^{(n+1)} = \eta(\nabla \boldsymbol{v}^{(n+1)} + (\nabla \boldsymbol{v}^{(n+1)})^{\mathrm{T}}) \tag{13}$$

where the bracketed superscript represents the time level. The vector functions $\boldsymbol{F}, \boldsymbol{C}, \boldsymbol{L}$ represent the semi-discrete representation of the time derivative of velocity, the nonlinear convection term and the remaining linear terms, respectively.

For the implicit Euler scheme, the vector functions take the following interpretations, where $\boldsymbol{m}$ is the velocity of the grid and $\boldsymbol{b}$ represents body forces:

$$\boldsymbol{F}_{(n+1),(n),(n-1)} = \boldsymbol{v}^{(n+1)} - \boldsymbol{v}^{(n)} \tag{14}$$

$$\boldsymbol{C}_{(n+1),(n),(n-1)} = (\boldsymbol{v}^{(n+1)} - \boldsymbol{m}) \cdot \nabla \boldsymbol{v}^{(n+1)} \tag{15}$$

$$\boldsymbol{L}_{(n+1),(n)} = \nabla \cdot \boldsymbol{\tau}^{(n+1)} - \nabla p^{(n+1)} + \mathbf{b}^{(n+1)} \tag{16}$$

Two Adams based schemes were considered. For the first Adams scheme, the linear terms, $\boldsymbol{L}$, were treated using the implicit second order Adams Moulton and the nonlinear convection, $\boldsymbol{C}$, treated using explicit second order Adams Bashforth. For the second Adams scheme, both the linear and nonlinear terms were treated using the implicit second order Adams Moulton scheme. For both Adams based schemes, the time derivative is as in the implicit Euler scheme (14).

For the second order Gear's method the time derivative, $\boldsymbol{F}$, is given by

$$\boldsymbol{F}_{(n+1),(n),(n-1)} = \tfrac{1}{2}(3\boldsymbol{v}^{(n+1)} - 4\boldsymbol{v}^{(n)} + \boldsymbol{v}^{(n-1)}) \tag{17}$$

with the other functions, $\boldsymbol{L}, \boldsymbol{C}$, given as for the Euler approach (15)–(16).

Typically, for a statically loaded journal bearing $\boldsymbol{m} = \mathbf{0}$. However, a non-zero value of $\boldsymbol{m}$ is employed in Section 9.2.1 as a verification exercise. Another reason for including a mesh velocity in the above equations is to facilitate the extension of the above scheme to the case of the dynamically loaded journal.

When the convection term, $\boldsymbol{C}$, is treated implicitly, the nonlinear scheme (11)–(13) is solved iteratively for $(p, \boldsymbol{v}, \boldsymbol{\tau})$ at time level $n+1$ using a simple Picard iteration scheme, which is described in the appendix. Each iteration involves the solution of a semi-discrete transient Stokes problem. In a number of cases an implicit treatment of the convection term is essential for numerical stability.

In practice, the number of such Picard iterations required to solve the semi-discrete system of Equations (11)–(13) at each time step is of the order of five. Only in extreme cases, such as when the journal lies very close to the bearing, did the scheme fail to converge. As expected, this implicit system is significantly more robust than the explicit approach in which the inertia term is computed at the previous time step. Furthermore, the scheme performed better than the popular operator integration factor splitting (OIFS) approach of Maday *et al.* [23] which is a second-order characteristics method.

We do not present results here regarding the comparison of the different transient discretization schemes. However, the Adams based schemes, for both the static and dynamically loaded journal, were significantly less robust than the backward Euler and second order Gear's method, often displaying spurious oscillatory behaviour. The Euler scheme provided the backbone to the development of the numerical algorithm and the second order Gear approach was chosen as the final transient discretization scheme for the fluid's governing equations.

5.2. *Spatial discretization*

The spectral element method is based on a weak formulation of the governing equations. The formulation of the problem is a combination of the three-field spectral element approach of Gerritsma and Phillips [24] and the variable viscosity model of Gwynllyw and Phillips [25]. The three-field formulation is implemented since it can be readily extended to viscoelastic flows and does not result in any significant increase in computational complexity when compared with the velocity–pressure formulation. Here we will give a brief description of the spectral element method for the generalized Newtonian fluid, using the pressure–velocity–stress formulation.

The weak form of the semi-discrete scheme (11)–(13) is as follows: Find $(\boldsymbol{v}, p, \boldsymbol{\tau}) \in X(\Omega) \times L_0^2(\Omega) \times Y(\Omega)$ such that

$$\int_\Omega (p \nabla \cdot \mathbf{w}) \, \mathrm{d}\Omega + \int_\Omega (\boldsymbol{\tau} : \nabla \cdot \mathbf{w}) \, \mathrm{d}\Omega + \frac{\rho}{\Delta t} \int_\Omega (\mathbf{w} \cdot \boldsymbol{v}) \, \mathrm{d}\Omega = \int_\Omega (\mathbf{w} \cdot \mathbf{f}) \, \mathrm{d}\Omega \quad \forall \mathbf{w} \in X(\Omega) \tag{18}$$

$$\int_\Omega (q \nabla \cdot \boldsymbol{v}) \, \mathrm{d}\Omega = 0, \quad \forall q \in L^2(\Omega) \tag{19}$$

$$\int_\Omega (\boldsymbol{\tau} : \mathbf{s}) \, \mathrm{d}\Omega + \int_\Omega 2\eta (\mathbf{s} : \nabla \boldsymbol{v}) \, \mathrm{d}\Omega = 0 \quad \forall \mathbf{s} \in Y(\Omega) \tag{20}$$

where we have dropped the time level $n+1$ from the superscript on $\boldsymbol{v}$, p and $\boldsymbol{\tau}$. Here

$$\mathbf{f} = \rho((\boldsymbol{v}^{(n)}/\Delta t) - (\boldsymbol{v}^{(n+1)} - \boldsymbol{m}) \cdot \nabla \boldsymbol{v}^{(n+1)}) + \mathbf{b}^{(n+1)}$$

and the various function spaces used in (18)–(20) are defined by

$$X(\Omega)=[H^1(\Omega)]^2,\quad Y(\Omega)=[L^2(\Omega)]^4_s,\quad L^2_0(\Omega)=\left\{\phi\in L^2(\Omega):\int_\Omega \phi\,\mathrm{d}\Omega=0\right\}$$

The stress space $Y(\Omega)$ is the space of symmetric 2×2 tensors whose components are square integrable over Ω.

The spectral element method is a technique for solving problems defined in complex geometries. In this method the computational domain is partitioned into several spectral elements. This decomposition of the domain is geometrically conforming in the sense that the intersection of two adjacent elements is either a common vertex or an entire edge. Each spectral element is mapped onto the parent element $D=[-1,1]^2$ using the transfinite mapping technique of Gordon and Hall [26]. The corresponding discrete weak formulation of the problem is constructed by replacing the integrals over each element by appropriate Gauss–Legendre quadrature rules. This procedure results in a system of linear equations for the primitive variables.

A two-dimensional Gauss–Lobatto Legendre grid with $(N+1)^2$ nodes is constructed over each spectral element which is mapped to the parent element. Each primitive variable is then approximated over the parent element using Legendre Lagrangian interpolants. For example, the velocity representation over the parent element is given by

$$\boldsymbol{v}^k_N(\xi,\zeta)=\sum_{i=0}^{N}\sum_{j=0}^{N}\boldsymbol{v}^k_{i,j}h_i(\xi)h_j(\zeta) \tag{21}$$

where $h_i:[-1,1]\to\mathbf{R}$ are Lagrangian interpolants on the Gauss–Lobatto Legendre collocation points and $\boldsymbol{v}^k_N$ is the discrete velocity field for the kth spectral element. Hence, the velocity field is chosen to be in $P_{N,K}$, the space of polynomials of degree N or less, defined over the K elements.

As for the finite element method, the velocity and pressure approximations must satisfy the Babuška-Brezzi condition to avoid the presence of spurious modes. In the framework of the spectral element method Maday and Patera [27] have shown that a suitable choice for the pressure approximation space is

$$M_N=L^2(\Omega)\cap P_{N-2,K} \tag{22}$$

The pressure nodes are chosen to be the interior Gauss–Lobatto Legendre points resulting in the following representation over the parent grid:

$$p^k_N(\xi,\zeta)=\sum_{i=1}^{N-1}\sum_{j=1}^{N-1}p^k_{i,j}\hat{h}_i(\xi)\hat{h}_j(\zeta) \tag{23}$$

where $\hat{h}_i:[-1,1]\to\mathbf{R}$ are Lagrangian interpolants on the interior Gauss–Lobatto Legendre collocation points and p^k_N is the discrete pressure field for the kth spectral element.

From the work of Gerritsma and Phillips [24], the components of the extra-stress tensor are chosen in $P_{N,K}$, and thus the extra-stress tensor has a representation of the form identical within the spectral element as that for the components of velocity

$$\boldsymbol{\tau}^k_N(\xi,\zeta)=\sum_{i=0}^{N}\sum_{j=0}^{N}\boldsymbol{\tau}^k_{i,j}h_i(\xi)h_j(\zeta) \tag{24}$$

Along an element interface, contiguous elements share common grid points and hence there are two unknowns associated with each component of velocity and extra-stress at such points. The values of these unknowns are forced to be the same for the velocity thus giving rise to a continuous velocity approximation. However, this is not done explicitly for the extra-stress which therefore allows for the possibility of discontinuous extra-stress approximations across element boundaries.

Test functions chosen from the appropriate subspaces of $X(\Omega)$, $L_0^2(\Omega)$ and $Y(\Omega)$ are used to generate the discrete system of equations. Combined with the iteration scheme described in the appendix, the results are a system of linear algebraic equations:

$$B\boldsymbol{\tau}_N - D^*\mathbf{p}_N - \sigma M\boldsymbol{v}_N = \mathbf{f}_N \tag{25}$$

$$D\boldsymbol{v}_N = \mathbf{g}_N \tag{26}$$

$$A\boldsymbol{\tau}_N - B^*\boldsymbol{v}_N = \mathbf{h}_N \tag{27}$$

where the subscript N in these equations indicates a vector of numerical values evaluated at the discretization points. Matrices B and D represent discrete divergence operators corresponding to extra-stress and velocity, respectively. In addition, $D^* = -D^{\mathrm{T}}$ and $B^* = -2VB^{\mathrm{T}}$, where V is the diagonal matrix with entries being the fluid viscosity, η, at the discretization points. The diagonal matrices M and A are the velocity and extra-stress mass matrices, respectively, and $\sigma = \rho/\Delta t$. The $\boldsymbol{v}_N$ vector does not contain values prescribed from the boundary conditions; contributions from the Dirichlet boundary conditions are placed in the right hand side of (26)–(27). Hence the vector $\mathbf{f}_N$ contains contributions from the Dirichlet boundary conditions, nonlinear convection term, the velocity at the previous time step and body forces, and the vectors $\mathbf{g}_N$ and $\mathbf{h}_N$ both contain contributions from the Dirichlet boundary conditions. Note that in order to evaluate the discrete gradient and divergence operators we need to map the pressure p_N and the test function q_N within each spectral element from the interior Gauss–Lobatto Legendre nodes onto the Gauss–Lobatto Legendre nodes on the boundary of the element.

Block Gaussian elimination yields a symmetric semi-positive definite system for the pressure unknowns

$$S\mathbf{p}_N = \mathbf{c}_N, \tag{28}$$

where

$$S = DE^{-1}D^*, \quad E = BA^{-1}B^* - \sigma M \tag{29}$$

and $\mathbf{c}_N = \mathbf{g}_N - DE^{-1}\mathbf{k}_N$ and $\mathbf{k}_N = \mathbf{f}_N - BA^{-1}\mathbf{h}_N$. Matrix A is diagonal and hence its inversion is trivial.

The matrix S is made positive definite by imposing a zero volume condition on the pressure field to eliminate its arbitrariness. The velocity is computed using

$$E\boldsymbol{v}_N = D^*\mathbf{p}_N + \mathbf{k}_N \tag{30}$$

and the discrete stress is evaluated by

$$A\boldsymbol{\tau}_N = B^*\boldsymbol{v}_N + \mathbf{h}_N \tag{31}$$

To summarize, the solution of (28), (30) and (31) in that order results in the numerical values for p_N, $\boldsymbol{v}_N$ and $\boldsymbol{\tau}_N$, respectively, at the discretization points. The method of solution for this system of linear equations is discussed in the next section.

5.3. *Solution of the linear system*

Due to the properties of S, an iterative solver for (28) is preferred. The nested preconditioned conjugate gradient (PCG) approach to solving systems of this type is well documented [28] and with the use of a suitable preconditioner the PCG method is found to be very efficient. However, for the journal bearing geometry, in which the physical aspect ratios can be large, the standard choice of preconditioner for the Stokes problem, i.e. the pressure mass matrix, is not robust [25].

For the case of the journal bearing, the pressure matrix S can be ill-conditioned due to the high aspect ratio of the geometry. For the $(p, \boldsymbol{v})$ formulation, condition numbers of the order of 10^8 have been computed [25]. The result is that, even for symmetric positive definite systems, the conjugate gradient algorithm fails to converge. Improved condition numbers have been computed for the $(p, \boldsymbol{v}, \boldsymbol{\tau})$ formulation but ill-conditioning problems are still encountered [29]. A solution to this problem, is to evaluate the inverse of the pressure matrix S using a direct method (such as Choleski decomposition), and to use that inverse as the preconditioner for the system. Of course, given the inverse of S one can obtain a solution to (28) by one simple matrix–vector product. However incorporating the direct inverse together with the PCG scheme does improve accuracy in the resulting solution with, typically, two iterations of PCG required to obtain a satisfactory solution of the ill-conditioned system. For time-dependent problems and a static geometry, this iterative improvement approach is inexpensive since the linear system needs to be solved a number of times with the preconditioner evaluated only once. A more detailed study of this iterative method with high aspect ratio spectral element grids is given in a recent paper [29]. A study of the accuracy of the resulting approximations and its relation to both physical and elemental aspect ratios is also presented in this article.

The problem under consideration in this paper, the dynamically loaded journal bearing, possesses an additional difficulty in that the movement of the grid needs to be determined and hence the pressure matrix S is altered at every time-step. In this paper the size of the time-step is kept constant, thereby avoiding the issue of the performance of preconditioners as a function of the time-step. Following previous work [25, 30] we propose using a preconditioner based on the inverse of the pressure matrix for a particular eccentricity ratio. Initially, the preconditioner will be the inverse of the pressure matrix at time $t = 0$. The performance of this preconditioner is monitored and, if it is deemed to become inefficient, a new preconditioner is generated, that being the inverse of the current pressure matrix.

6. MESH MOVEMENT

This section describes the moving grid approach to the spectral element method as required for the dynamically loaded journal bearing system. The algorithm for evaluating the motion of the journal will be described later. Two approaches are considered for the moving grid, namely a quasi-Eulerian approach (QE) and an arbitrary Lagrangian–Eulerian approach (ALE). In both approaches, the physical grid moves continuously with the motion of the journal in such a manner that the position of any grid point is a function of the eccentricity and attitude angle

of the journal. The choice of this function has a bearing on the efficiency of the numerical scheme. As a result of this grid generation, the motion of any grid point is a function of its position and the motion of the centre of the journal. Hence the motion of a grid point is independent of the fluid's velocity at that grid point.

6.1. *Quasi-Eulerian* (*QE*)

This subsection describes the quasi-Eulerian approach to the dynamic journal bearing problem, an approach that has been successfully employed in a number of publications (see, for example, References [30–32]).

With the motion of a grid point defined we now have the concept of the velocity of a grid point. The QE scheme makes the assumption that the velocities of all the grid points are small in magnitude so that an Eulerian approach can be employed. That is, the partial time derivative of the fluid velocity is approximated by

$$\frac{\partial \boldsymbol{v}}{\partial t} \approx \frac{\delta \boldsymbol{v}}{\delta t} \tag{32}$$

where $\delta \boldsymbol{v}/\delta t$ is the referential time-derivative with respect to the moving grid. The simplest finite difference approximation of this derivative is given by

$$\left.\frac{\delta \boldsymbol{v}}{\delta t}\right|^{(n+1)} \approx \frac{\boldsymbol{v}^{(n+1)} - \boldsymbol{v}^{(n)}}{\Delta t} \tag{33}$$

where $\boldsymbol{v}^{(n+1)}$, $\boldsymbol{v}^{(n)}$ are the fluid velocities evaluated at the same (moving) physical grid point at consecutive time steps.

The QE scheme is simple to implement. Furthermore, for transient Stokes flow, there are no convection terms, thus making the resulting computation more efficient. On the negative side, the QE scheme imposes a limit on the grid velocity which is not quantified. The current work will report that the grid generation constraints imposed on QE can lead to preconditioning and accuracy problems. These difficulties will be discussed in more detail in Sections 9.2.1 and 9.2.2, respectively. Although not studied in this paper, the inclusion of cavitation into the lubricant model introduces further constraints on a moving mesh [33] which may be beyond the limitations of the QE scheme.

6.2. *Arbitrary Lagrangian–Eulerian* (*ALE*)

A more sophisticated approach to evaluating the partial time derivative within a moving grid system is the arbitrary Lagrangian–Eulerian (ALE) approach. In the ALE formulation the reference system is considered as a computational reference system, which can be chosen quite arbitrarily. Given a reference frame with velocity $\boldsymbol{m}$ then the partial time derivative can be evaluated by

$$\frac{\partial}{\partial t} = \frac{\delta}{\delta t} - (\boldsymbol{m} \cdot \nabla) \tag{34}$$

where $\delta/\delta t$ is the time derivative with respect to the moving reference frame. When the reference frame is fixed ($\boldsymbol{m} = 0$) the Eulerian description is recovered. When the reference frame follows the motion of the fluid ($\boldsymbol{m} = \boldsymbol{v}$) the Lagrangian description is recovered with $\delta/\delta t$ becoming the material derivative.

In this paper, the reference frame is taken to be the spectral element grid which is determined at each time step by the position of the journal. With this approach, the evaluation of the numerical approximation to $\delta/\delta t$ requires no interpolation. In addition, and unlike the QE approach, no assumptions are made regarding the grid velocity. The extra convection term introduced in the ALE scheme is absorbed into the iterative temporal scheme described in Section 5.1 with $\boldsymbol{m}$ evaluated analytically given the velocity and position of the centre of the journal.

7. MOTION OF JOURNAL

In terms of the journal bearing, two distinct systems are considered in this paper, namely the DLJ and the JBS as described in the introduction.

For the DLJ system, the motion of the journal is calculated by integrating

$$m\ddot{\mathbf{r}} = \boldsymbol{F} \quad \text{where} \quad \boldsymbol{F} = \boldsymbol{R} + \boldsymbol{S} \tag{35}$$

with $\boldsymbol{R}$ being the hydrodynamic force on the journal and $\boldsymbol{S}$ being the prescribed applied load; typically the force applied by a piston. The hydrodynamic force, $\boldsymbol{R}$, is evaluated through the Cauchy stress tensor by

$$\boldsymbol{R} = -\int_{\Gamma_J} \boldsymbol{\sigma} \cdot \hat{\boldsymbol{n}} \, \mathrm{d}s \tag{36}$$

where $\hat{\boldsymbol{n}}$ is the outward unit normal to Γ_J, respectively.

The journal bearing simulator is a system whereby the journal's path is prescribed. In this paper the JBS model is used to analyse and compare the numerical schemes. In experiments, the JBS has proved useful in investigating lubricant behaviour, such as cavitation and reaction forces, within a dynamic environment [34]. A schematic diagram of the JBS system is given in Figure 2.

The numerical stability of the motion of a dynamically loaded journal bearing can be very sensitive to the mass of the journal. Not unexpectedly this was particularly relevant when using the forward Euler formula in the evaluation of the motion of the journal [30]. In using such an explicit scheme, the applied load of the journal ($\boldsymbol{F}$) is evaluated at each time step in the semi-discrete representation. Double integration of (35), using the forward Euler method, results in a new journal velocity and position being evaluated. The existence of a journal mass threshold, beneath which the numerical evaluation of the journal's path is unconditionally unstable, is explained in Reference [13]. In the current work, an implicit approach is employed to determine the path of the journal in order to improve its numerical stability properties. As for the momentum equation, a number of different schemes were considered for the time integration to evaluate the motion of the journal. These implicit schemes were the backward Euler scheme, Adams–Moulton scheme and the 2nd order Gear's method. The approach adopted for the backward Euler is as follows, with the straightforward alteration to implement the other methods:

$$\text{Given } \mathbf{r}^{(n)}; \quad \mathbf{r}^{(n+1)} = \mathbf{r}^{(n)} + \Delta t \cdot \boldsymbol{v}_J^{(n+1)}; \quad \boldsymbol{v}_J^{(n+1)} = \boldsymbol{v}_J^{(n)} + \Delta t \cdot \boldsymbol{F}^{(n+1)}/m \tag{37}$$

where $\mathbf{r}$ is the position vector of the journal's centre, $\boldsymbol{v}_J$ the journal's translational (squeeze) velocity, $\boldsymbol{F}$ is the applied load on the journal, m is the mass of the journal and the superscripts refer to the time stage at which these variables are evaluated.

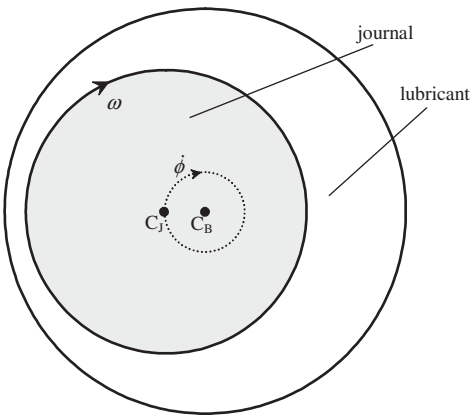

Figure 2. Schematic illustration of the JBS system. The journal rotates about its own axis with angular velocity ω and, in addition, the centre of the journal rotates about the centre of the bearing with angular velocity $\dot{\phi}$.

The roots of the implicit equations (37) are found using a Newton–Raphson scheme to calculate $\boldsymbol{F}^{(n+1)}$ and $\boldsymbol{v}^{(n+1)}$. In our computations, this rarely required more than six iterations to converge to an acceptable tolerance. We underline that within each iteration of the Newton–Raphson scheme for the motion of the journal, there nests a Picard iteration scheme to solve the implicit Navier–Stokes system.

As expected the use of an implicit approach has a very significant effect on the numerical stability of the evaluation of the journal's locus. Results presented later on the stabilizing effect of inertia on the journal bearing would not have been possible using the forward Euler approach described in [30]. As for its application to the fluid equations, the Adams–Moulton scheme again displayed oscillatory behaviour which was removed by using a smaller time-step. Both the backward Euler and 2nd order Gear's method were robust in their application to tracking the motion of the journal with the higher order Gear's method being the preferred choice.

8. GRID GENERATION

In order to compare the QE and ALE approaches to the spectral element journal bearing simulation we will describe two different spectral element grids that were employed in our investigation. In both grid generating algorithms the position of the inter-elemental boundaries uniquely defines the grid. Therefore, the two algorithms differ only in their positioning of the inter-elemental boundaries. To be more precise, they differ only in the positioning of the radial inter-elemental boundaries. The differences are listed as follows:

1. Grid-A: radial inter-elemental boundaries congruent to the centre of the journal.
2. Grid-B: radial inter-elemental boundaries congruent to the centre of the bearing.

Typical grids generated from these two algorithms, for identical positioning of the journal, are illustrated in Figures 3 and 4. As can be seen from Figure 4, Grid-B is valid only if the diameter of the journal is greater than the radius of the bearing, which is certainly the case in typical engineering journal bearings.

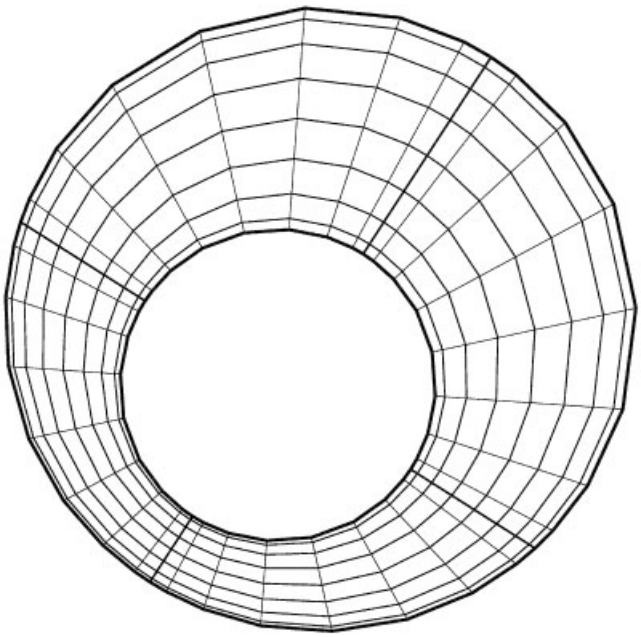

Figure 3. Grid-A: Spectral element grid with radial lines congruent at the centre of the journal.

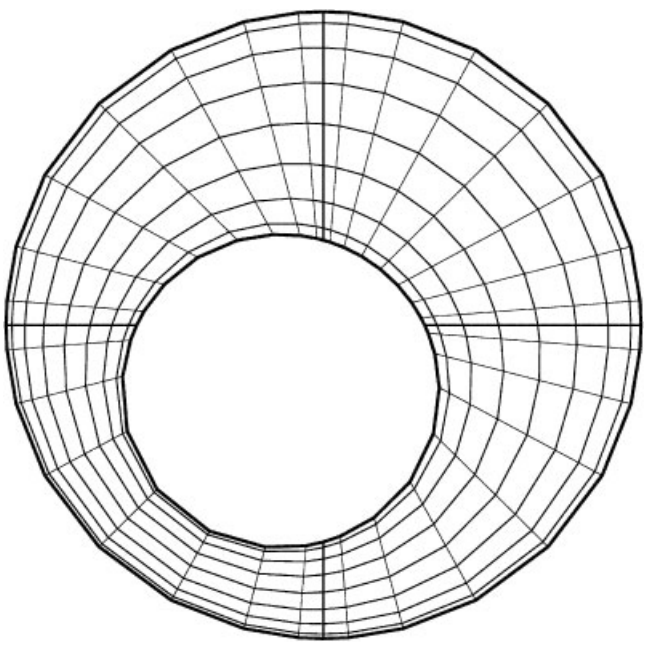

Figure 4. Grid-B: Spectral element grid with radial lines congruent at the centre of the bearing. Alignment of the radial lines are independent of the position of the centre of the journal.

The algorithm for generating the grids is described as follows:

1. Select Grid-A or Grid-B which will determine the point of congruency, given by C, of the radial lines.
2. Insert radial inter-elemental boundaries. They will be distributed evenly in the azimuthal direction. In the case of Grid-B, one of the inter-elemental boundaries will pass through the centre of the bearing.
3. Insert the inner radial lines. For each spectral element, they will be distributed in the azimuthal direction according to Gauss–Lobatto Legendre distribution.
4. Insert azimuthal inter-elemental boundaries of which one will be the bearing and one will be the journal. These inter-elemental boundaries are circles, the centres of which lie on the line joining the journal and the bearing. The radii and positions of the centres of these circles are evenly distributed.
5. Insert the inner azimuthal lines, each one being circular. For each spectral element, each line will have its centre and radius distributed according to Gauss–Lobatto Legendre distribution.

9. NUMERICAL RESULTS

9.1. Performance of preconditioners

9.1.1. Fixed grid. As an illustration of the requirement to use a preconditioner to solve (28), consider the modelling of a statically loaded journal bearing lubricated by a Newtonian fluid with the parameters given in Table I.

For the purpose of this exercise the transient algorithm is executed using, as initial conditions on $\boldsymbol{v}$, a zero velocity field except on the journal's surface where the boundary conditions (5) are enforced. The number of PCG iterations is recorded at each time step until steady state is reached. A relative tolerance of 10^{-8} on the pressure field is used as the convergence criterion for the PCG algorithm at each time step. The solution (pressure) vector at the previous time step is used as the initial solution vector for each execution of the PCG algorithm.

This section will compare the performance of different preconditioners. We consider separately the use of preconditioners for a system with uniform viscosity and one with variable viscosity. In all the results presented the arbitrariness of the pressure system is removed by

Table I. Basic parameters used in comparing the performance of different preconditioners for the outer PCG solver of the Uzawa system (28).

Bearing radius (m)	0.03129
Journal radius (m)	0.03125
Eccentricity ratio	0.5
Viscosity (Pa s)	5×10^{-3}
(N_r, N_a, E_r, E_a)	(8,8,1,2)
Density (kg/m^3)	875
Angular velocity (rads/s)	500

the introduction of a zero-pressure volume constraint [25] weighted to an extent that minimizes κ_p where κ_p is the condition number of the preconditioned system. The chosen weighting is dependent upon the time step.

9.1.2. Uniform viscosity. Using the system parameters defined in Table I the performance of five different preconditioners are considered in conjunction with the PCG algorithm for solving the Uzawa system (28). These preconditioners, P, are as follows:

$$\text{(i) } P = S_{0.5}, \quad \text{(ii)} P = S_{0.25}, \quad \text{(iii) } P = S_0, \quad \text{(iv) } P = D(S_{0.5}), \quad \text{(v) } P = I$$

where S_ε is the coefficient matrix of the Uzawa system (28) resulting from an eccentricity ratio of ε with uniform viscosity. The matrix function D returns the diagonal of the matrix argument and I is the identity matrix.

Two different time steps are considered, namely $\Delta t = 10^{-4}$ and $\Delta t = 10^{-6}$.

- $\Delta t = 10^{-4}$
  Figure 5 illustrates the number of PCG iterations required for the first 20 time-steps. In conjunction with this figure, Table II lists the condition number, κ_P, of the corresponding preconditioned system, $Q^{-1}SQ^{-\mathrm{T}}$, where P is the preconditioner, S is the system matrix (28) and $P = QQ^{\mathrm{T}}$.
- $\Delta t = 10^{-6}$
  Figure 6 illustrates the number of PCG iterations required for the first 400 time steps, sampled every ten time-steps. In conjunction with this figure, Table III lists the condition number, κ_P, of the corresponding preconditioned system, $Q^{-1}SQ^{-\mathrm{T}}$.

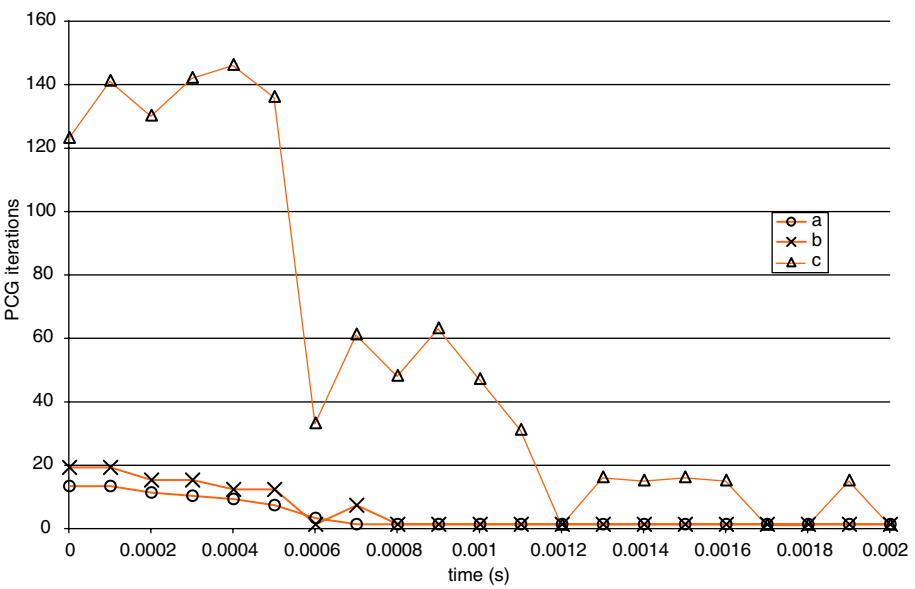

Figure 5. Number of PCG iterations for different preconditioners with $\Delta t = 10^{-4}$ and uniform viscosity. Preconditioners used are as follows: (a) $P = S_{0.25}$; (b) $P = S_0$; and (c) $P = D(S_{0.5})$. Note: the case of $P = I$ failed to converge to the required tolerance.

Table II. The condition number, κ_P, of the preconditioned system, $Q^{-1}SQ^{-\mathrm{T}}$, for different preconditioners.

P	κ_P
$S_{0.5}$	1
$S_{0.25}$	2.13×10^4
$S_{0.0}$	3.09×10^5
$D(S_{0.5})$	1.01×10^8
I	2.40×10^8

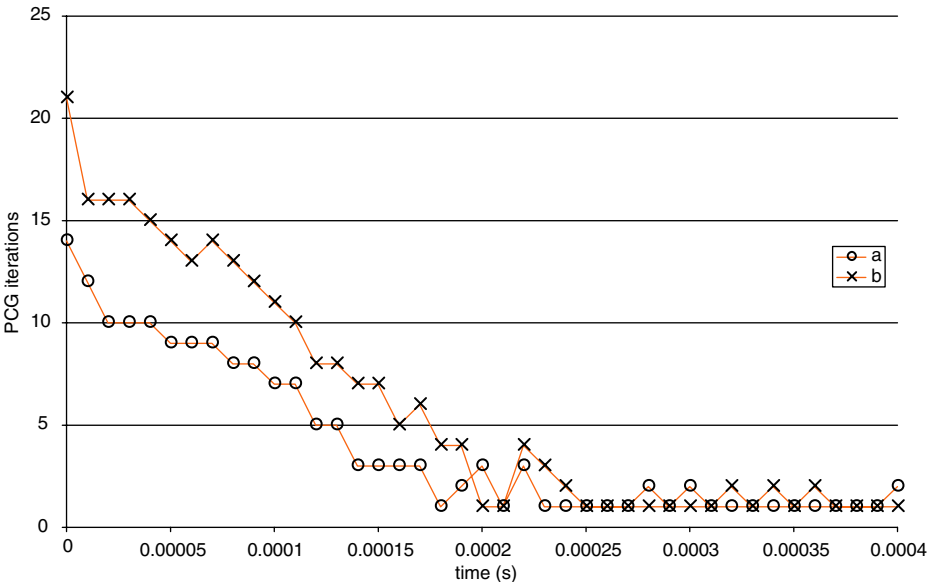

Figure 6. Number of PCG iterations for different preconditioners with $\Delta t = 10^{-6}$ and uniform viscosity. Preconditioners used are as follows: (a) $P = S_{0.25}$; and (b) $P = S_0$. Note: the case of $P = I$ and $P = D(S_{0.5})$ failed to converge to the required tolerance.

Table III. κ_P, the condition number of the preconditioned system, $Q^{-1}SQ^{-\mathrm{T}}$, for different preconditioners.

P	κ_P
$S_{0.5}$	1
$S_{0.25}$	6.41×10^6
$S_{0.0}$	1.00×10^8
$D(S_{0.5})$	1.35×10^9
I	2.16×10^9

The condition number of the preconditioned system, is significantly higher for the smaller time-step which results in the inability of $P = D(S_{0.5})$ to converge to the required tolerance. However, the differences in κ_P between the two time-steps is not reflected in the performances of either of the two preconditioners $P = S_{0.25}$, $P = S_0$. The decreasing time step results in the increased domination of the mass matrix within the matrix E defined in (29). We will not investigate the reason why the increased domination by the mass matrix results in increased condition numbers for certain preconditioners. The poor conditioning of the Uzawa operator S (29) is due to the poor conditioning of DD^* [29].

9.1.3. Variable viscosity. Variable viscosity in this paper is considered through the Barus relation, given by

$$\eta = \eta_0 e^{\beta p} \tag{38}$$

where p is the pressure of the fluid, β is the Barus parameter and η_0 is the fluid's viscosity at atmospheric pressure. Such fluids are also known as piezoviscous fluids. Here we take $\eta_0 = 5 \times 10^{-3}$ for comparison with the case of uniform viscosity and $\beta = 3 \times 10^{-8}$. With the exception of viscosity, all parameters are as listed in Table I. The time step is taken to be $\Delta t = 10^{-5}$. As in the uniform viscosity case, the initial conditions are those of zero velocity field. The viscosity of the fluid at a given time is evaluated through its pressure at the previous time step.

Unlike the uniform viscosity case, the Uzawa operator will vary with time due to the variation of viscosity in time. The preconditioners used here incorporate the zero pressure condition and hence assume a uniform viscosity profile. On reaching steady state the fluid's maximum/minimum viscosities are 5.97×10^{-3} and 4.27×10^{-3} Pa s, respectively.

Figure 7 illustrates the number of PCG iterations required for the first 50 time-steps, sampled every ten time steps. In conjunction with this figure, Table IV lists the condition numbers, κ_P^i, κ_P^s of the corresponding preconditioned system at the initial and final (steady state) time steps.

The introduction of variable viscosity produces a moderate change in κ_P when using $P = S_{0.5}$ as the fluid moves from the stationary initial condition to the steady state. The second time step produces the greatest transient change in η. From then on, the number of iterations decreases to unity as a result of the initial vector in the PCG iteration being the solution vector at the previous time step.

9.1.4. Moving grid. The main reason that Grid-A was originally implemented in Reference [30] was due to the fact that, with this grid, the resulting Uzawa operator is not a function of the attitude angle of the journal (ϕ in Figure 1). Hence, in the case of the JBS, where the eccentricity of the journal is fixed, the Uzawa operator does not vary with time, thus significantly reducing computation time in terms of matrix construction and inversion. Even in the case of the dynamically loaded journal bearing, the variation of the journal's eccentricity is often small compared to the variation in its attitude angle. Therefore, in using Grid-A for the dynamically loaded journal bearing, the system matrices are often *slowly varying* resulting in a preconditioner of the PCG iteration scheme that is efficient over a large number of time steps. An efficient preconditioner is essential for solving such a system due to the large

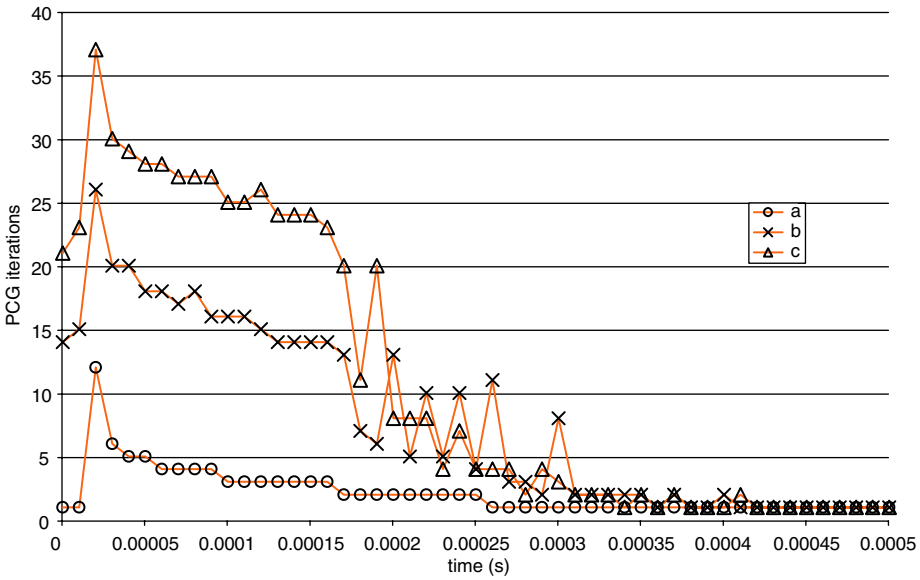

Figure 7. Number of PCG iterations for different preconditioners with $\Delta t = 10^{-5}$ and variable viscosity. Preconditioners used are as follows: (a) $P = S_{0.5}$; (b) $P = S_{0.25}$; and (c) $P = S_0$. Note: the case of $P = I$ and $P = D(S_{0.5})$ failed to converge to the required tolerance.

Table IV. κ_P^i, κ_P^s, the condition numbers of the preconditioned system, $Q^{-1}SQ^{-\mathrm{T}}$, for different preconditioners. κ_P^i is the condition number at the first time-step and κ_P^s the condition number at the final time step (steady state).

P	κ_P^i	κ_P^s
$S_{0.5}$	1	1.38
$S_{0.25}$	1.42×10^5	1.43×10^5
$S_{0.0}$	2.18×10^6	2.18×10^6

number of time steps and the poor conditioning of the Uzawa operator in geometries with large aspect ratios.

In contrast to Grid-A, the implementation of Grid-B results in the Uzawa operator being a function of both the eccentricity and the attitude angle of the journal. The result is that, for the JBS, the Uzawa operator varies with time. As a comparison of the efficiency of the two grids, Figure 8 shows the number of PCG iterations for the JBS system using Grid-B. The system parameters are given in Table VI. The preconditioner employed here is the direct inverse of the system matrix (28) for the initial geometry. Also plotted in this figure is $|10\sin(\phi)|$ which illustrates the relationship between the number of iterations and the attitude angle of the journal. Since the JBS system matrix does not vary when Grid-A is used, the number of PCG iterations for this grid remains at unity throughout the computation. For

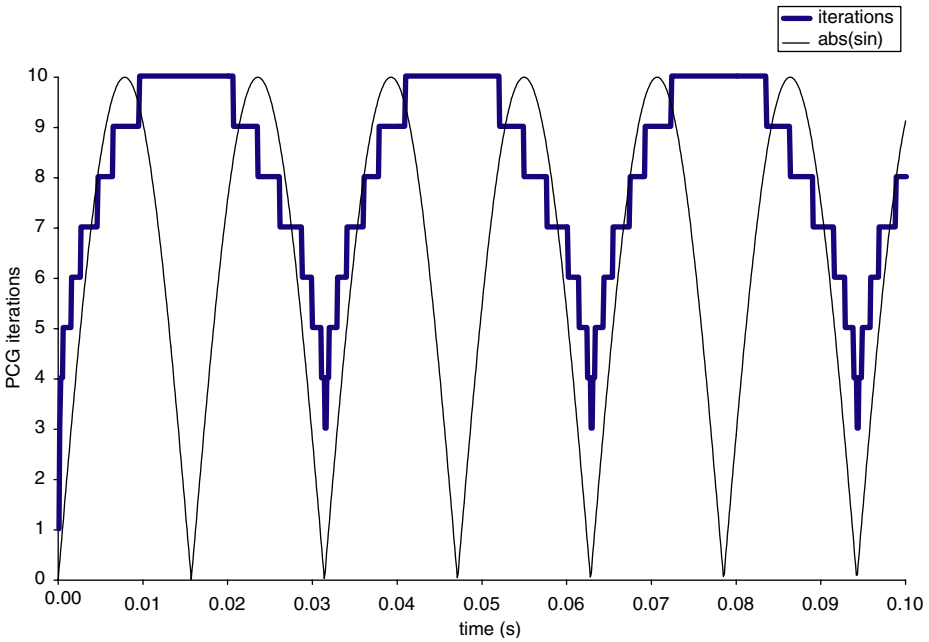

Figure 8. Number of PCG iterations for the Grid-B formulation plotted against time. Also included is a plot of $|10\sin(\phi)|$.

the Grid-B formulation, the number of PCG iterations clearly varies with the attitude angle of the journal, with the maximum number of iterations (ten) corresponding approximately to the region $\phi \in (2n+1)\pi \pm \pi/3$. In the figure, the first complete cycle of the journal occurs at time $t = 0.0314$.

9.2. *Comparison of QE and ALE*

This section concentrates on the comparison between the QE approach employed initially in Reference [30] and the ALE approach. We start with a consistency test followed by a comparison of the two methods applied to the JBS problem. Finally we make a comparison of the two methods for the dynamically loaded journal bearing.

9.2.1. Consistency test. For the purpose of performing a consistency test a grid is generated in an artificial manner. Note that this is not implemented in any of the practical applications of the schemes.

The verification test involves a statically loaded journal bearing system which is initially at steady state. The Grid-A spectral element grid is then moved azimuthally around the statically loaded journal. It is only the grid that is moving, and hence the steady state results should be preserved. This process is illustrated schematically in Figure 9 with the radial elemental boundaries rotating about the fixed centre of the journal.

The parameters used in this verification exercise are listed in Table V. This journal bearing system supports a hydrodynamic force of $(F_x, F_y) = (-24.7, 1.13 \times 10^5)N$. Here (F_x, F_y) are the

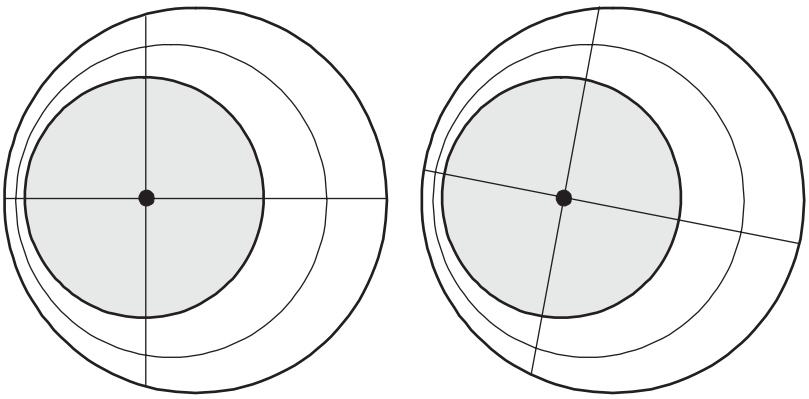

Figure 9. Schematic illustration of the grid movement for the consistency test. Journal is statically loaded whilst the radial part of the spectral element grid rotates clockwise about the centre of the journal. The right hand figure shows the grid at a later time to the left hand figure.

Table V. Table of parameters used in the verification and comparison exercises between QE and ALE.

Bearing radius (m)	0.03129
Journal radius (m)	0.3125
Eccentricity ratio	0.1
Journal angular velocity (rad/s)	200
Grid angular velocity (rad/s)	10
Density (kg/m^3)	100
Viscosity (Pa s)	5×10^{-3}

Cartesian components of the hydrodynamic force. The effect of rotating the spectral element grid upon F_x is illustrated in Figure 10. In this figure, F_x is plotted against time and the predictions of the QE and ALE schemes are compared. The domain of the graph (0.7 s) is slightly longer than the period of the rotation of the grid (0.63 s). In preserving the steady state value of F_x, the ALE approach is clearly more accurate than the QE approach. These results correspond to a grid angular velocity of 10 rad/s. Increasing the grid angular velocity further results in even greater variation in F_x for the QE approach whilst ALE preserves the uniform value of $-24.7N$. The former observation is due to an increased departure from the QE assumption that the grid velocity is small.

As far as the dominant Cartesian force component, F_y, is concerned, both the ALE and QE approaches preserve the value of $F_y = 1.13 \times 10^5 N$ as the grid rotates. Since the variation in the magnitude of the hydrodynamic force vector is small, even for the QE scheme, the above result should be taken as a verification of the ALE approach as opposed to a criticism of the QE scheme for this grid velocity. However, in using the QE scheme, care must be taken with the grid velocity and its effect on the results being analysed.

9.2.2. Journal bearing simulator (*JBS*). The journal bearing simulator (JBS) system is described in Section 7. In this section we consider the motion of such a system in which the

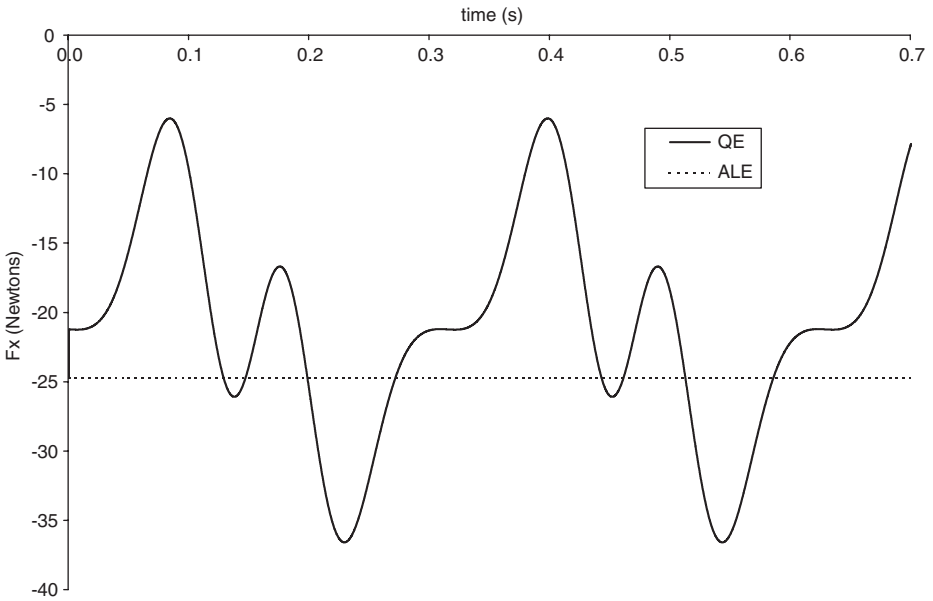

Figure 10. Comparison of the horizontal force component, F_x, between the QE and ALE schemes for a statically loaded journal bearing with rotating spectral element grid. System parameters are given in Table V.

Table VI. Table of parameters used for the JBS system.

Bearing radius (m)	0.0300
Journal radius (m)	0.0295
Eccentricity ratio	0.1
ω (rad/s)	0
$\dot{\phi}$ (rad/s)	200
Density (kg/m^3)	800
Viscosity (Pa s)	5×10^{-3}

centre of the journal traces a circular locus about the centre of the bearing and the journal simultaneously rotates about its own centre. This motion is illustrated schematically in Figure 2 where the angular velocity of the journal about its own centre is represented by ω and the angular velocity of the journal's centre about the bearing's centre is represented by $\dot{\phi}$.

The predictions of the ALE and QE schemes are compared for the JBS system. As part of the comparison, the two grid generation algorithms, Grid-A and Grid-B, are considered.

The parameters for the JBS system considered in this section are given in Table VI.

Three different combinations of grid generation algorithms with moving grid methodologies are considered in this section, namely:

(i) QE using Grid-A (QE-A),
(ii) QE using Grid-B (QE-B),
(iii) ALE using Grid-A.

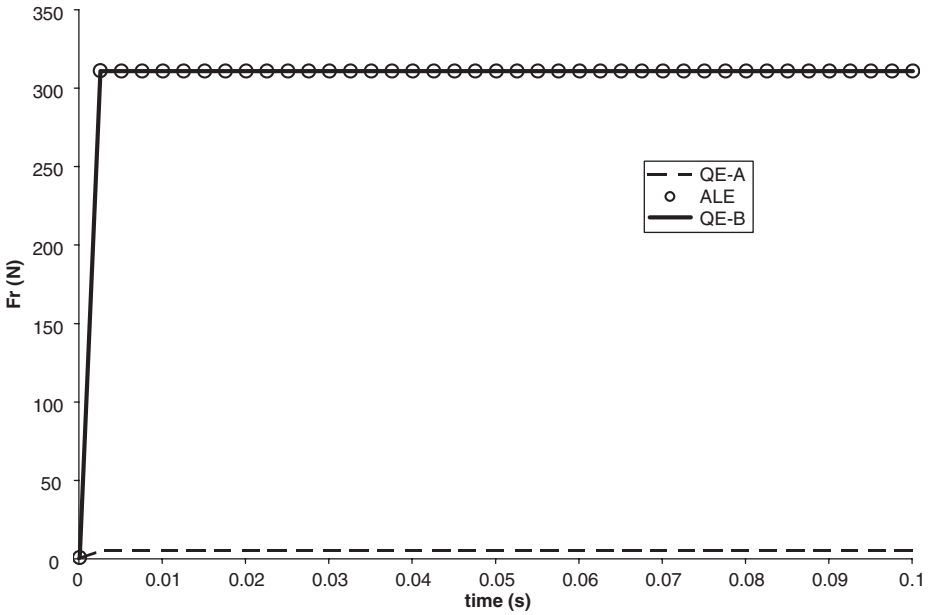

Figure 11. Comparison of the radial component of the hydrodynamic force, F_r, in a JBS system using: (i) QE-A; (ii) QE-B; and (iii) ALE. System parameters are given in Table VI.

ALE using Grid-B is not considered since Grid-B was specifically designed for the QE scheme in order to preserve the assumptions of a slowly moving grid. Grid-B has the disadvantage of being more expensive in terms of PCG iterations (see Section 9.1.4). The slowly moving grid assumption is not required for ALE, and hence we deem that ALE is better suited to the more efficient Grid-A approach.

A comparison is made between the hydrodynamic forces obtained from these three schemes applied to the JBS system. The results are shown in Figures 11 and 12 which display the (F_r, F_t) components of the hydrodynamic forces, respectively. Figure 12 shows that all three methods (i)–(iii) agree reasonably well for the tangential component of the hydrodynamic force, F_t, with the differences in the results being about 1.5%. However, in the computations of the radial component of the hydrodynamic force, F_r, as shown in Figure 11, QE-B and ALE are in close agreement, but differ significantly from the results of QE-A. The agreement here forms a validation exercise for ALE using the faster Grid-A when compared with the application of the QE approach to the slower moving, but less efficient, Grid-B. Furthermore, the result of QE-A indicates that Grid-A is unsuitable in this application of the QE scheme since the higher mesh velocity results in a loss of accuracy.

This section and Section 9.1.4 have highlighted some advantages and disadvantages of implementing Grid-A and Grid-B into the QE approach. With the faster moving grid, QE-A is more efficient than QE-B due to the ϕ-independent property of the system matrix. The cost of this advantage is a loss of accuracy. In contrast the ALE approach possesses all of the listed advantages of these methods and none of the disadvantages. The above results therefore justify the implementation of ALE for moving spectral element journal bearing systems.

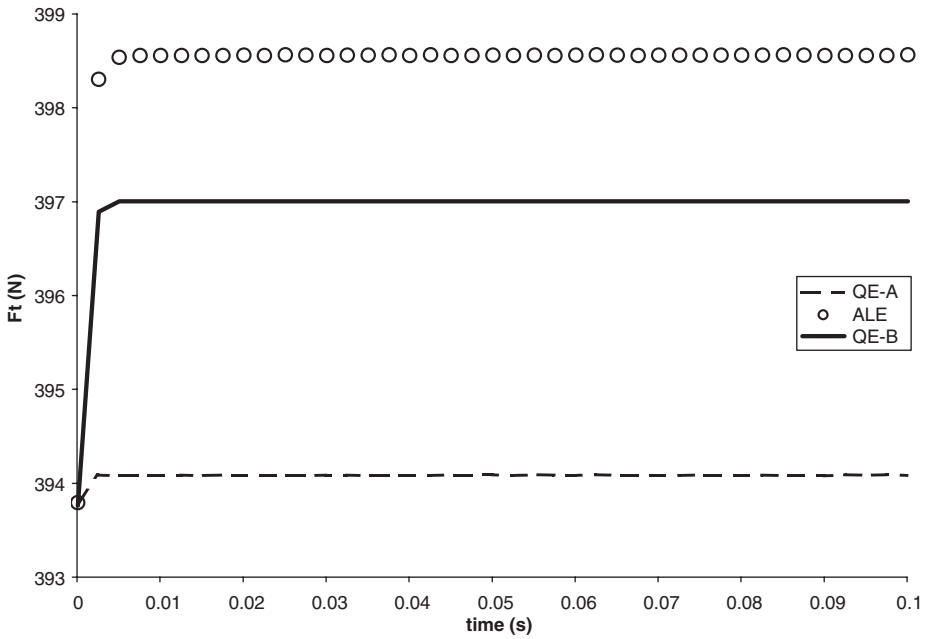

Figure 12. Comparison of the tangential component of the hydrodynamic force, F_t, in a JBS system using: (i) QE-A; (ii) QE-B; and (iii) ALE. System parameters are given in Table VI.

Next, we consider the dynamically loaded system which includes a comparison of the ALE approach with that of using QE-A, the latter method having been used in numerous papers on the dynamically loaded journal bearing (see, for example References [30–32]).

9.2.3. Dynamically loaded journal bearing. In Section 9.2.2, comparing the ALE and QE methods for the JBS system, we highlighted the difference between the two methods. In order to obtain good agreement between the QE and ALE methods there is a necessity for the QE method to have a slowly moving grid. When this constraint is violated, as in the case of the QE-A system, it is not difficult to obtain examples for the dynamically loaded journal bearing (DJB) for which there are significant differences between the QE and ALE methods. On the other hand, for numerous DJB systems for which the journal is physically stable, such as tending towards a steady state, only small differences between the ALE and QE-A methods are noted. The main reason for this is that, for a journal system that tends towards steady state (and hence zero translational velocity for the journal) the spectral element mesh velocity will also tend towards zero.

With physically stable journals that produce limit cycles for the path of the journal, the observed differences between QE-A and ALE are small once the limit cycle is obtained. Again, the mesh velocities observed in such DJB systems are significantly lower than those observed in JBS systems. These observations support the use of the QE-A approach to modelling dynamically loaded journal bearings. However, it has to be noted that in some publications (for example Reference [33]), the QE method was used to model a cavitating dynamically

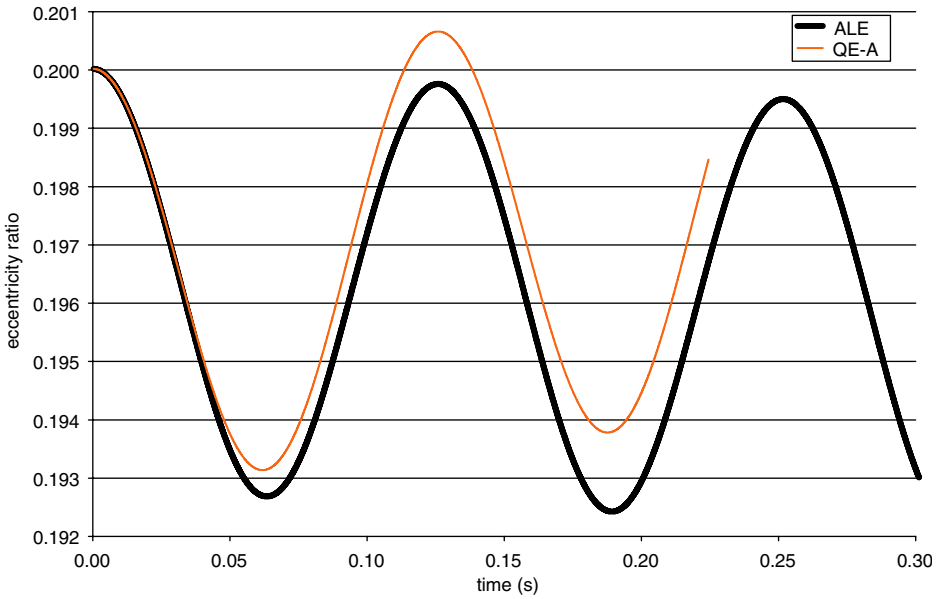

Figure 13. Comparison of eccentricity ratio between the ALE and QE-A schemes for a DLJ system. The journal's initial position is given by $(\varepsilon, \phi) = (0.2, 0)$. Other parameters are given in Table VII.

loaded journal bearing system. In such a model, the stability of the numerical algorithm was enhanced by the inter-elemental boundaries following the boundary of the cavitating fluid. In such a case it may be possible that the velocity of the moving mesh may be too high for the QE methodology to be accurately implemented. In all of the DJB systems considered in this paper (Section 9.3) no limit cycle contained the origin. If such a system was considered, then the QE-A approach would result in the radial spectral elements completing a full cycle about the centre of the journal. The result would be a higher grid velocity than those encountered in this paper and therefore not necessarily suitable for the QE method.

An additional justification for implementing ALE for the DJB system is illustrated in Figure 13 for a system containing inertia. This figure compares the eccentricity ratio with time for computations made by using ALE and by using the QE-A approach. The system's parameters are given in Table VII. Lubrication theory predicts that the journal will tend towards a steady state: the steady state being well inside the initial position of the journal. From the figure it is clear that ALE predicts a journal with an overall decreasing eccentricity whilst the QE-A approach suggests that the journal will be physically unstable. The same parameters as in this comparison are used in the next section when comparing with lubrication theory.

Even for an inertialess fluid, for which the ALE approach is typically five times slower than the QE-A approach, it is still recommended to use the ALE approach as the influence of the mesh velocity on the accuracy of QE-A is somewhat unpredictable and therefore results in a less robust scheme.

Table VII. Parameters for the comparison between lubrication theory and ALE, which results in a physically stable system. Results using these parameters are supplied in Figures 13 and 14.

Bearing radius (m)	0.05005
Journal radius (m)	0.05000
ω (rad/s)	500
Density (kg/m^3)	400
Viscosity (Pa s)	5×10^{-3}
Journal mass (kg)	184
Prescribed applied load (N)	1800

9.3. Comparison of ALE and lubrication theory

In previous sections, we have described the dynamically loaded journal bearing (DJB) system (Section 7), the ALE approach using spectral elements (Sections 5 and 6.2) and lubrication theory applied to the DJB system (Section 4).

This section will present and compare the results of using the spectral element method with ALE and lubrication theory for modelling the DJB system.

The parameters that contribute to a physically more stable system through the effects of inertia demand finer numerical discretizations than for a physically unstable system. This is not the case for a system that is physically stable through, for example, the effects of a pressure thickening fluid. For the spectral element method, the finer spatial and temporal granularity due to increased inertia effects is significantly more demanding than for the one-dimensional lubrication theory approach.

For this reason we shall present only one comparison between the ALE approach and lubrication in which the resulting physical system is stable due to the effect of inertia. The parameters used in such a run are given in Table VII.

Due to computational expense, the results for ALE are only presented up to time $t = 1$. The eccentricity ratios presented in Figure 14 are those for the lubrication theory and for the spectral element/ALE approach. Two results are presented for the ALE approach, namely those obtained when using the backward Euler method and Gear's method for tracking the journal locus. The results presented are accurate to graphical tolerance for the lubrication theory and the spectral element approach when using Gear's method. To achieve this accuracy a time step of $\Delta t = 10^{-5}$ s and spatial parameters of $(N_r, N_a, E_r, E_a) = (10, 10, 1, 2)$ were used for Gear's method and a time step of $\Delta t = 2.5 \times 10^{-6}$ s for the lubrication theory. The numerical parameters used for the backward Euler's method for the ALE approach is the same as that for Gear's method; the results from Euler's method have not achieved graphical tolerance.

The figure illustrates the close agreement for this system between lubrication theory and the ALE approach using Gear's method. A time step of less than $\Delta t = 10^{-6}$ s would have been required to obtain similar results using the backward Euler approach. At start-up in the ALE method a much smaller time-step was required in order to preserve convergence of the nested iterations of the inertia solver (see the Appendix) and the journal locus solver (37). After a few time-stages, however, the quoted time step of $\Delta t = 10^{-5}$ s was sufficient to preserve numerically accurate results.

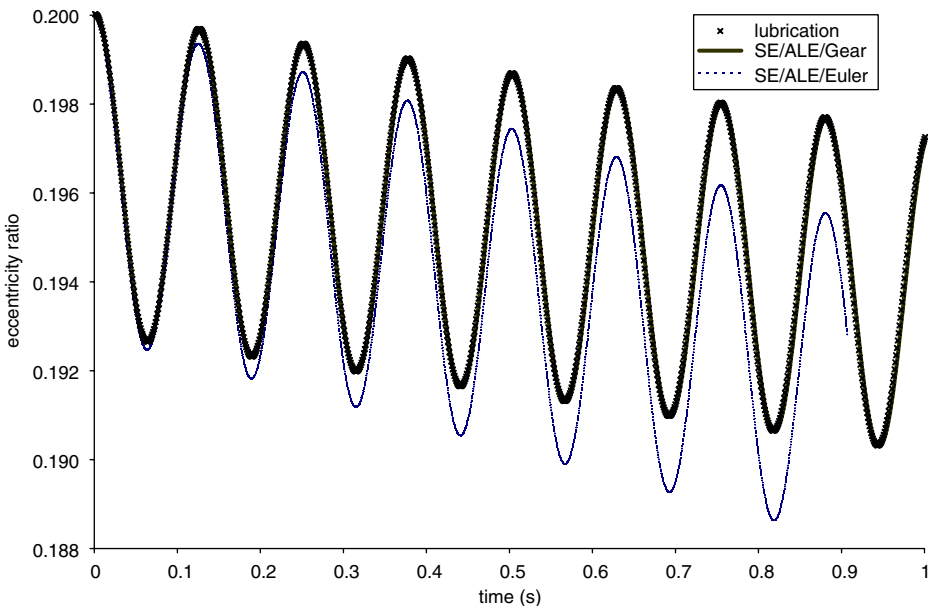

Figure 14. Comparison of eccentricity ratio evaluated using lubrication theory and ALE. The journal's initial position is given by $(\varepsilon, \phi) = (0.2, 0)$. Other system parameters are given in Table VII. The results for the lubrication theory and Gear's method are almost indistinguishable.

Table VIII. Parameters for the comparison between lubrication theory and ALE, which results in a physically unstable system. Results using these parameters are supplied in Figures 15 and 16.

Bearing radius (m)	0.03129
Journal radius (m)	0.3125
ω (rad/s)	250
Density (kg/m^3)	800
Viscosity (Pa s)	5×10^{-3}
Journal mass (kg)	5×10^4
Prescribed applied load (N)	5×10^5

The above results are over a relatively short time frame for this journal bearing system. Applying lubrication theory to this system over a long time frame (>100 s) results in the journal arriving at a small stable limit cycle near the origin with a maximum eccentricity ratio of approximately 7×10^{-3}. In order to achieve this limit cycle using the ALE approach within a reasonable time, we would have to set the journal's initial position to be close to the limit cycle.

We now consider a less computationally demanding scenario in which to compare ALE and lubrication theory in a system that is physically unstable. The parameters used in such a run are given in Table VIII.

The geometry of this problem has a very small gap which suggests that it is a suitable geometry for analysis by lubrication theory. Figures 15 and 16 compare the journal locus for

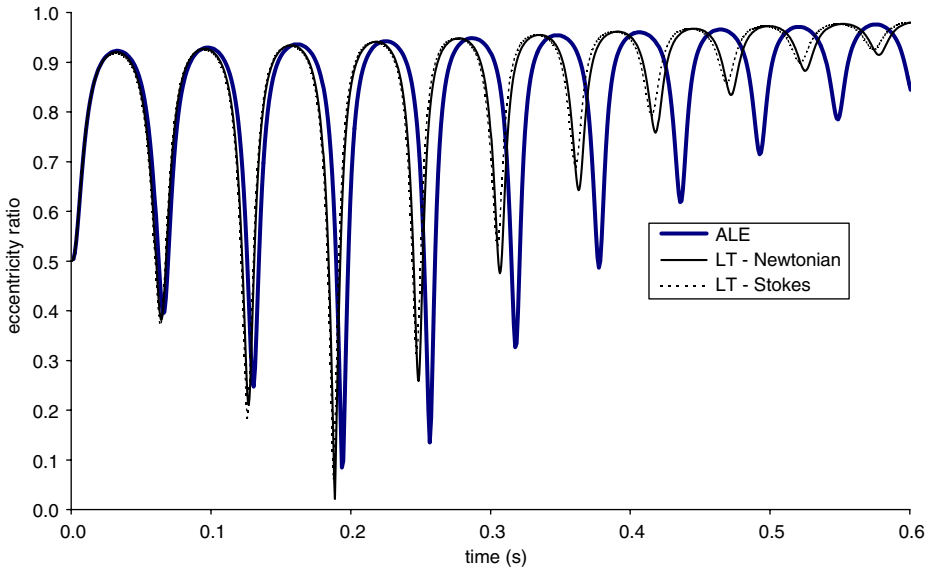

Figure 15. Comparison of eccentricity ratio evaluated using lubrication theory (LT) (Newtonian and Stokes) and ALE. The journal's initial position is given by $(\varepsilon, \phi) = (0.5, 0)$. Other system parameters are given in Table VIII.

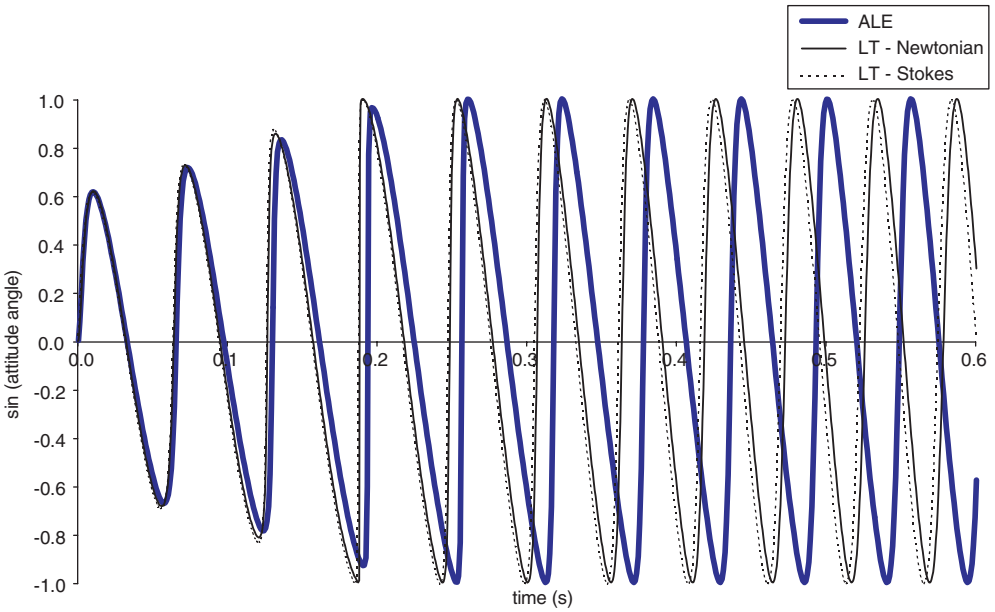

Figure 16. Comparison of sin ϕ evaluated using lubrication theory (LT) (Newtonian and Stokes) and ALE. The journal's initial position is given by $(\varepsilon, \phi) = (0.5, 0)$. Other system parameters are given in Table VIII.

the parameters listed in Table VIII using (i) ALE for a Newtonian lubricant, (ii) lubrication theory for a Newtonian lubricant and (iii) lubrication theory for a Stokes lubricant. The results in these figures are accurate to graphical tolerance, using $\Delta t = 2.5 \times 10^{-6}$ s for both ALE and lubrication theory, and $(N_r, N_a, E_r, E_a) = (10, 10, 1, 2)$ for ALE.

All three paths differ significantly although the influence of inertia on the lubrication theory path is the least significant. All three models display the property of tending towards half-speed whirl. The most striking difference between the methods is in the plot for the eccentricity ratio where, within one period of motion of the journal about the centre of the bearing, the minimum eccentricity of the ALE method is much lower than predicted by lubrication theory. The corresponding maximum eccentricities are much more in agreement.

The attitude angles of the three models are similar in shape but there are significant phase shifts between them. Again the most significant difference is between the ALE and lubrication theory for the Newtonian fluid with lubrication theory predicting a comparatively small inertial effect on the attitude angle. This example highlights the failure of lubrication theory to model the dynamics accurately.

10. CONCLUDING REMARKS

In this paper issues regarding the construction and movement of spectral element meshes using an ALE formulation have been considered within the framework of journal bearing lubrication. The lubricant in this study is modelled using a generalized Newtonian model in which a Barus law is used to describe the dependence of viscosity on pressure.

A comparison between the predictions of lubrication theory and direct numerical simulations using the spectral element method has shown that although the former is more efficient than the latter, since it is based on an approximation of the latter, it cannot be universally relied upon to provide accurate results. In particular, the lubrication approximation fails to capture the dynamics of the journal accurately when inertial effects are important. Furthermore, the direct numerical simulation approach facilitates the inclusion of more refined mathematical models such as those derived from kinetic theory considerations (see Phillips and Smith [35], for example).

The discrete equations at each time step are solved using the PCG method in which the most efficient preconditioner is one that is allowed to change in a dynamic fashion. The preconditioner is based on a Choleski decomposition of the Uzawa operator evaluated at a given journal eccentricity. The use of an implicit time-stepping technique to compute the path of the journal is essential for the spectral element method. The range of journal mass for which numerically stable results are possible is far greater than when an explicit time-stepping approach was used.

Issues concerning the generation and movement of spectral element meshes form the focus of this paper. In particular, comparisons between the QE and ALE methodologies have been performed. The influence of the magnitude of the mesh velocity on the performance of these methods has been investigated and shown to have a profound effect on the range of validity of the QE approach. On the contrary, the ALE formulation is not subject to such severe constraints on the movement of the mesh and is therefore extremely robust.

APPENDIX A: ITERATIVE SOLVER FOR THE NONLINEAR CONVECTION TERM

System $L(n+1, m+1)$:

$$\rho\left(\frac{\boldsymbol{v}^{(n+1,m+1)}-\boldsymbol{v}^{(n)}}{\Delta t}+(\boldsymbol{v}^{(n+1,m)}-\boldsymbol{m})\cdot\nabla\boldsymbol{v}^{(n+1,m)}\right)=\nabla\cdot\boldsymbol{\tau}^{(n+1,m+1)}-\nabla p^{(n+1,m+1)} \tag{A1}$$

$$\nabla\cdot\boldsymbol{v}^{(n+1,m+1)}=0 \tag{A2}$$

$$\boldsymbol{\tau}^{(n+1,m+1)}=\eta(\nabla\boldsymbol{v}^{(n+1,m+1)}+(\nabla\boldsymbol{v}^{(n+1,m+1)})^{\mathrm{t}}) \tag{A3}$$

Picard iteration procedure performed at each time stage $(n+1)$:

begin

$m := 0$

$\boldsymbol{v}^{(n+1,m)} := \boldsymbol{v}^{(n)}$

do while (not converged)

Solve $L(n+1, m+1)$ for $\boldsymbol{v}^{(n+1,m+1)}, \boldsymbol{\tau}^{(n+1,m+1)}, p^{(n+1,m+1)}$

$m := m+1$

If $\boldsymbol{v}^{(n+1,m)} \approx \boldsymbol{v}^{(n+1,m-1)}$ then converged

end do

$\boldsymbol{v}^{(n+1)} := \boldsymbol{v}^{(n+1,m)}$

end

ACKNOWLEDGEMENTS

One of the authors (D.Rh.G.) is grateful for the support of the Nuffield Foundation via their New Lecturers initiative.

REFERENCES

1. Hirt CW, Amsden AA, Cook JL. An arbitrary Lagrangian–Eulerian computing method for all flow speeds. *Journal of Computational Physics* 1974; **14**:227–253.
2. Noh WF. A time-dependent two-space dimensional coupled Eulerian–Lagrangian code. In *Methods in Computational Physics 3*, Adler B, Fernbach S, Rotenberg M (eds). Academic Press: New York, 1964; 117–179.
3. Donea J, Giuliani S, Halleux JP. An arbitrary Lagrangian–Eulerian finite element method for transient dynamic fluid-structure interactions. *Computer Methods in Applied Mechanics and Engineering* 1982; **33**:689–723.
4. Belytschko T, Kennedy JM, Schoeberie DF. Quasi-Eulerian finite element formulation for fluid structure interaction. *ASME Journal of Pressure Vessel Technology* 1980; **102**:62–69.
5. Hughes TJR, Hulbert GM. Space–time finite element methods for elasto-dynamics: formulations and error estimates. *Computer Methods in Applied Mechanics and Engineering* 1988; **66**:339–363.
6. Tezduyar TE, Liou J, Behr M. A new strategy for finite element computations involving moving boundaries and interfaces—the DSD/ST procedure. I. The concept and the preliminary numerical tests. *Computer Methods in Applied Mechanics and Engineering* 1992; **94**:339–351.
7. Tezduyar TE, Liou J, Behr M, Mittal S. A new strategy for finite element computations involving moving boundaries and interfaces—the DSD/ST procedure. II. Computation of free-surface flows, two-liquid flows, and flows with drafting cylinders. *Computer Methods in Applied Mechanics and Engineering* 1992; **94**:353–371.
8. Behr M, Tezduyar TE. Finite element solution strategies for large-scale flow simulations. *Computer Methods in Applied Mechanics and Engineering* 1994; **112**:3–24.
9. Glowinski R, Pan TW, Hesla TI, Joseph DD. A distributed Lagrangian multiplier/fictitious domain method for particulate flows. *International Journal of Multiphase Flow* 1999; **25**:755–794.

10. Succi S. *The Lattice Boltzmann Equation*. Oxford University Press: Oxford, 2001.
11. Hu HH, Joseph DD, Crochet MJ. Direct simulation of fluid particle motions. *Theoretical and Computational Fluid Dynamics* 1992; **3**:285–306.
12. Hu HH. Direct simulation of flows of solid–liquid mixtures. *International Journal of Multiphase Flow* 1996; **22**:335–352.
13. Hu HH, Patankar NA, Zhu MY. Direct numerical simulations of fluid–solid systems using the arbitrary Lagrangian–Eulerian technique. *Journal of Computational Physics* 2001; **169**:427–462.
14. Ho LW, Patera AT. A Legendre spectral element method for simulation of unsteady incompressible viscous free-surface flows. *Computer Methods in Applied Mechanics and Engineering* 1990; **80**:355–366.
15. Ho LW, Patera AT. Variational formulation of three-dimensional viscous free-surface flows: natural imposition of surface tension boundary conditions. *International Journal for Numerical Methods in Fluids* 1991; **13**: 691–698.
16. Davies AR, Li XK. Numerical modelling of pressure and temperature effects in viscoelastic flow between eccentrically rotating cylinders. *Journal of Non-Newtonian Fluid Mechanics* 1994; **54**:331–350.
17. Barnes HA, Hutton JF, Walters K. *An Introduction to Rheology*. Elsevier: Amsterdam, 1989.
18. Bates TW, Williamson B, Spearot JA, Murphy CK. A correlation between engine oil rheology and oil film thickness in engine journal bearing. Society of Automotive Engineers 1986, *Technical Report 860376*.
19. Paranjpe RS. Analysis of non-Newtonian effects in dynamically loaded finite journal bearings including mass conserving cavitation. *Transactions of the ASME* 1992; **114**:736–746.
20. Taylor RI. The inclusion of lubricant shear thinning in the short bearing approximation. *Proceedings of the Institute of Mechanical Engineers*, *Part J*: *Journal of Engineering Tribology* 1999; **213**:35–46.
21. Zhang C. TEHD behaviour of non-Newtonian dynamically loaded journal bearings in mixed lubrication for direct problem. *Journal of Tribology*, *Transactions of the ASME* 2002; **124**:178–185.
22. Collins D, Savage MD, Taylor CM. The influence of fluid inertia on the stability of a plain journal bearing incorporating a complete oil film. *Journal of Fluid Mechanics* 1986; **168**:415–430.
23. Maday Y, Patera AT, Rønquist EM. An operator-integration-factor splitting method for time-dependent problems: application to incompressible fluid flow. *SIAM Journal on Scientific Computing* 1990; **5**:263–292.
24. Gerritsma MI, Phillips TN. Discontinuous spectral element approximations for the velocity–pressure–stress formulation of the Stokes problem. *International Journal for Numerical Methods in Engineering* 1998; **43**: 1401–1419.
25. Gwynllyw DRh, Phillips TN. Preconditioned iterative methods for unsteady non-Newtonian flow between eccentrically rotating cylinders. *SIAM Journal on Scientific Computing* 1996; **40**:1239–1266.
26. Gordon WJ, Hall CA. Construction of curvilinear coordinate systems and applications to mesh generation. *International Journal for Numerical Methods in Engineering* 1973; **7**:461–477.
27. Maday Y, Patera AT. Spectral element methods for the incompressible Navier–Stokes equations. In *State of the Art Surveys in Computational Mechanics*, Noor AK, Oden JT (eds). ASME: New York, 1989; 71–143.
28. Maday Y, Meirion A, Patera AT, Rønquist EM. Analysis of iterative methods for the steady and unsteady Stokes problem: application to spectral element discretizations. *SIAM Journal on Scientific Computing* 1993; **14**:310–337.
29. Gwynllyw DRh, Phillips TN. On the enforcement of the zero mean pressure condition in the spectral element approximation of the Stokes problem. *Computer Methods in Applied Mechanics and Engineering*, 2004, submitted.
30. Gwynllyw DRh, Davies AR, Phillips TN. A moving spectral element approach to the dynamically loaded journal bearing problem. *Journal of Computational Physics* 1996; **123**:476–494.
31. Scales LE, Davies AR, Gwynllyw DRh, Li XK, Phillips TN, Williamson BP. The effect of lubricant rheology on the performance of dynamically loaded journal bearings. Society of Automotive Engineers 1997, *Technical Report 973002*.
32. Davies AR, Li XK, Phillips TN. The effect of viscoelasticity on the performance of dynamically loaded journal bearings. In *Proceedings of the XIIIth International Congress in Rheology*, Binding DM, Hudson NE, Mewis J, Piau J-M, Petrie CJS, Townsend P, Wagner MH, Walters K (eds). British Society of Rheology: Glasgow, 2000; 205–207.
33. Gwynllyw DRh, Davies AR, Phillips TN. On the effects of a piezoviscous lubricant on the dynamics of a journal bearing. *Journal of Rheology* 1996; **40**:1239–1266.
34. Bates TW, Roberts GW, Oliver DR, Milton AL. A journal bearing simulator bench test for ranking lubricant load-bearing capacity. Society of Automotive Engineers 1992, *Technical Report 922353*.
35. Phillips TN, Smith KD. A spectral element approach to the simulation of viscoelastic flows using Brownian configuration fields. *Journal of Non-Newtonian Fluid Mechanics*, 2004, submitted.

